

Cite this: *Nanoscale Adv.*, 2023, 5, 6405Received 12th October 2023  
Accepted 31st October 2023

DOI: 10.1039/d3na00880k

rsc.li/nanoscale-advances

# High conversion continuous flow exfoliation of 2D MoS<sub>2</sub>†

Thaar M. D. Alharbi<sup>ab</sup> and Colin L. Raston<sup>id</sup>\*<sup>b</sup>

We report a low-cost and highly efficient process for exfoliating of MoS<sub>2</sub> using an energy efficient vortex fluidic device (VFD). This method is high in green chemistry metrics in avoiding the use of auxiliary substances, and the process is scalable, with a conversion of as received MoS<sub>2</sub> into 2D sheets at ~73%.

Following the discovery of graphene with its almost limitless applications, attention has recently focused on other two-dimensional (2D) nanomaterials such as transition metal dichalcogenides (TMDs) due also to their unique electronic, optical, optoelectronic, mechanical and catalytic properties.<sup>1,2</sup> Of these, molybdenum disulfide (MoS<sub>2</sub>) is one of the most investigated. The crystal structure of MoS<sub>2</sub> consists of sandwiched layers of S–Mo–S with strong covalent bonding in each layer and weak van der Waals interactions between neighbouring layers, and thus there is potential exfoliation of the 2D material.<sup>3,4</sup> Indeed exfoliation of bulk MoS<sub>2</sub> into few-layered and individual monolayer sheets is crucial for use in a variety of applications. For this, a simple and scalable fabrication technique is required. To date, a variety of approaches have been explored, which include but not limited to liquid phase exfoliation, intercalation, solid state mechanical exfoliation, and chemical vapor deposition.<sup>5–7</sup> The above-mentioned methods for preparing such material, which are under batch processing, have some shortcomings including poor control of the exfoliation and difficulty in scaling up. Solid state mechanical exfoliation or liquid-phase exfoliation usually produces nanosheets with a rather broad size distribution and/or are formed in low yield. Intercalation driven exfoliation is time-consuming involving a number of steps.<sup>8</sup> Chemical vapor deposition to

generate 2D MoS<sub>2</sub> operates at high temperature with the material deposited on specific substrates, for example SiO<sub>2</sub>.<sup>9</sup> Coleman *et al.* have established the use of shear forces in liquids in a commercial kitchen blender to exfoliate MoS<sub>2</sub> in the presence of a surfactant as a large-scale process.<sup>10</sup> In a similar way, also in the presence of a surfactant, a rotating packed bed is effective in exfoliating MoS<sub>2</sub> into 2D material.<sup>11</sup> Yuan *et al.* used a high-shear mixer to exfoliate MoS<sub>2</sub> in a mixture of ethanol/water, with 30% conversion after 10 cycles of shearing.<sup>12</sup>

Avoiding the use of surfactants in the exfoliating process is important in generating pristine materials for then direct use in applications. It is also important to avoid the need for multistep processing and to be able to generate the 2D material in high yield, at the same time being able to readily scale up. To this end we have explored the use of the high shear stress generated within thin films of liquid in the vortex fluidic device (VFD) to exfoliate MoS<sub>2</sub> in the absence of surfactants or other auxiliary substances including toxic chemicals, while operating at room temperatures and under continuous flow conditions.<sup>13</sup> The choice of solvent for use in this thin film processing platform was a mixture of water and ethanol as an environmentally acceptable liquid. For context, the VFD imparts mechanical energy within liquids in the form of high shear topological fluid flows which have submicron diameters normal to the surface of the tube.<sup>13,14</sup> We find that the VFD is effective for high yielding exfoliation of MoS<sub>2</sub> into thin sheets. In a recent study we reported the use of the VFD in converting bulk MoS<sub>2</sub> into scrolls of the 2D material, with the active edges showing high activity towards the electrocatalytic hydrogen evolution reaction, but this required a different solvent system,<sup>15</sup> noting that different liquid systems behave differently in the VFD depending on their properties.<sup>13,14</sup>

Fig. 1 illustrates exfoliating of MoS<sub>2</sub> from bulk material using a VFD housing a standard quartz tube with a hemispherical base, 20 mm in diameter (17.5 mm internal diameter) and 18.5 cm in length. The hemispherical base generates a Coriolis in the thin film of liquid in the form of a spinning top (ST) or

<sup>a</sup>Physics Department, Faculty of Science, Taibah University, Almadinah Almunawarrah, 42353, Saudi Arabia

<sup>b</sup>Flinders Institute for Nanoscale Science and Technology, College of Science and Engineering, Flinders University, Adelaide SA 5001, Australia. E-mail: colin.raston@flinders.edu.au

† Electronic supplementary information (ESI) available. See DOI: <https://doi.org/10.1039/d3na00880k>



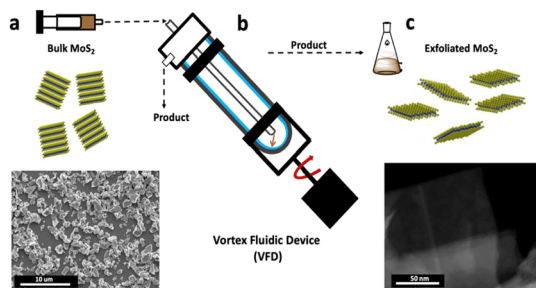


Fig. 1 Schematic of the experimental procedure for VFD exfoliating MoS<sub>2</sub>. (a) Bulk MoS<sub>2</sub> dispersed in a 1 : 1 mixture of ethanol/water with its SEM image before processing. (b) The device operating under continuous flow (rotational speed 8k rpm), MoS<sub>2</sub> concentration 5 mg mL<sup>-1</sup>, at a flow rate 0.45 mL min<sup>-1</sup> and tilt angle 45°. (c) STEM image of exfoliated MoS<sub>2</sub> nanosheets after VFD processing.

typhoon like high shear topological fluid flow, with Faraday wave eddies twisted into double helical (DH) flows running across the film of liquid of uniform thickness.<sup>13,14</sup> The diameter of the ST increases as the rotational speed increases whereas the diameter of the DH flows decreases, with the lateral force from the ST hypothesised to be driving the exfoliation process. The processing involved systematically exploring the use of different solvents and mixtures of solvents, and using different concentrations, Fig. S2–4.† A competing process is the simultaneous exfoliation and scrolling of the 2D material, which was optimal for a 1 : 1 : 1 mixture of DMF, water and ethanol, using the same size as received MoS<sub>2</sub> particles, as in the present study.<sup>15</sup> However, this was only effective in high yield for the VFD operating under confined mode. Scroll formation is mechanically understood by the scrolls being generated within the uplifting flow of the ST, which occurs at lower rotational speeds in the device, ~4k rpm, where the diameter of this part of the ST is small, forcing the 2D sheets into scrolls as they pass through,

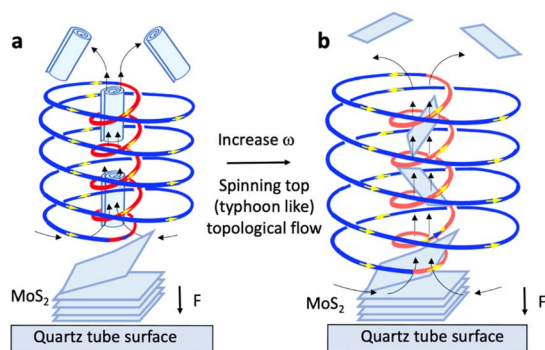


Fig. 2 Proposed mechanism of exfoliation of MoS<sub>2</sub> controlled by the spinning top (ST) (typhoon like) Coriolis force from the base of the VFD tube, with lateral forces on the surface of the particles and uplift within the core of the ST.<sup>12,13</sup> (a) Exfoliation with scrolling at 4k rpm (low speed) arising from inner ST compression on the exfoliated sheets as they are drawn into the ST. (b) ST topological fluid flow exfoliation on the surface of MoS<sub>2</sub> particles at 8k rpm (high speed) with the 2D sheets drawn into the core of the larger inner and outer diameter ST without compression.

Fig. 2a. At higher rotational speed, notably 8k rpm, the outside and internal diameters of the spinning top are larger, as established using molecular drilling experiments.<sup>13</sup> Here the exfoliated material passes through the spinning top without compression and associated scroll formation.

We established the optimum conditions for exclusively exfoliating MoS<sub>2</sub> (*i.e.* no scroll formation) as follows: as received bulk MoS<sub>2</sub> powder was dispersed in a mixture of ethanol and water in a volume ratio of 1 : 1, at a concentration 5 mg mL<sup>-1</sup>. Black solutions of dispersed MoS<sub>2</sub> were sonicated for 30 min and then injected into the base of the VFD tube rotating at 8k rpm and tilted at 45°, with the system operating at room temperature and the flow rate set at 0.45 mL min<sup>-1</sup>, noting that this flow rate is optimal for a number of continuous flow processes in the device.<sup>16,17</sup> The choice of solvent in the present study for exfoliating MoS<sub>2</sub> in forming thin sheets in high yield was critical. Different solvents were explored, at the optimised rotational speed herein (8k rpm), including NMP, DMF and ethanol, with no exfoliation evident, as shown in Fig. S2.† In addition, the concentration of MoS<sub>2</sub> was varied, using 2, 5 and 10 mg mL<sup>-1</sup>, as detailed in Fig. S3,† with exfoliation of 2D sheets at 5 mg mL<sup>-1</sup> being deemed optimal.

At high rotational speed, the diameter of the inner flow of the ST is too large to compress the exfoliated sheets into scrolls, Fig. 2a, *i.e.* the high shear ST topological fluid flow striking the surface of the MoS<sub>2</sub> provides the lateral force for exfoliating the material, Fig. 2b, with the 2D sheets able to pass through the larger inner diameter of the ST relative to that at lower rotational speed. We note that the mechanical energy bearing down on the surface of the tube can melt bismuth particles (mp 271.4 °C) for the VFD operating at room temperature, with the molten metal flowing up through the spinning top where it solidifies.<sup>13</sup> Thus, the mechanical energy is creating localised heating as well as lateral shear on the layers of MoS<sub>2</sub> at the liquid interface with MoS<sub>2</sub> particles themselves centrifugally held against the surface of the tube. Exposure to such forcing conditions collectively facilitates the exfoliation, although contact electrification may also be involved.<sup>17–19</sup> At high rotational speeds the ST is several microns in diameter and any exfoliated sheets drawn into the uplifting inner part of the spinning top, Fig. 2b, are not confined in space to create scrolls, Fig. 2a. In this context, the optimal conditions for creating MoS<sub>2</sub> scrolls is at low rotational speed, 4k rpm, where the outside diameter of the maximum shear stress bearing down on the tube surface ST is smaller than that at higher rotational speeds. The small inner up flow of the ST is responsible for the formation of scrolls, and this occurs in a 1 : 1 : 1 mixture of water, ethanol and DMF.<sup>15</sup> Exfoliation in the VFD has previously been reported for other 2D materials, notably of graphene from graphite, hexagonal boron nitride,<sup>20,21</sup> and phosphorene,<sup>22</sup> albeit without an understanding of the mechanism of their formation. The findings herein now provide an understanding of the mechanism of exfoliating 2D MoS<sub>2</sub> without spontaneous formation of scrolls, potentially as a general model for exfoliating 2D materials in the VFD. Theoretical studies on exfoliating graphene from graphite established that once scrolling of a graphene sheet passing the edge of the sheet contacting itself, then scrolling becomes



energetically favourable.<sup>23</sup> Presumably this also applies to the conversion of MoS<sub>2</sub> sheets into scrolls.

The exfoliated MoS<sub>2</sub> nanosheets were characterized using SEM, TEM, STEM and AFM, XRD and XPS. Fig. 3a presents SEM image at low magnification of exfoliated MoS<sub>2</sub>. The initial concentration of the bulk materials was 5 mg mL<sup>-1</sup>, and after processing in the VFD, the final concentration of exfoliated nanosheets was found to be 4.9 mg mL<sup>-1</sup> thus giving a high yield of ~73%, as can be observed from SEM in using a continuous flow process. TEM was used to further investigate the detailed structure of MoS<sub>2</sub> nanosheets. Fig. 3b and c shows TEM and HRTEM images of the same material, establishing that the exfoliated nanosheets are extremely thin, being transparent in the SEM, and overlying on each other. HRTEM was used to gain more insight into the structure of the exfoliated MoS<sub>2</sub> nanosheets formed in the VFD, as shown in Fig. 3c, establishing that the exfoliated MoS<sub>2</sub> has a *d*-spacing of 0.27 nm. This was directly measured from the HRTEM image and is consistent with *d* spacing of hexagonal MoS<sub>2</sub> (100) planes.<sup>24,25</sup> Fig. 3d–f displays STEM images along with the elemental mapping of the exfoliated MoS<sub>2</sub> nanosheets. The HAADF image in Fig. 3d establishes that the exfoliated MoS<sub>2</sub> is very thin. In addition, the elemental mapping of the exfoliated MoS<sub>2</sub> nanosheets established the presence of Mo and S throughout the exfoliated layer, Fig. 3e and f. Atomic force microscopy (AFM) was used to investigate the thickness and the lateral size of the exfoliated MoS<sub>2</sub> nanosheets. Fig. 4a and b shows the topography image of the exfoliated MoS<sub>2</sub> nanosheets associated with its height profile, with the thickness distributions and lateral size of the exfoliated sheets being ~2 nm and 700 nm respectively, Fig. 4c and d, which is indicative of the formation of monolayer and few layer sheets of MoS<sub>2</sub>.<sup>26,27</sup> Changing the size of the particles of the as received MoS<sub>2</sub> had minimal impact on the exfoliation process, Fig. S5.†

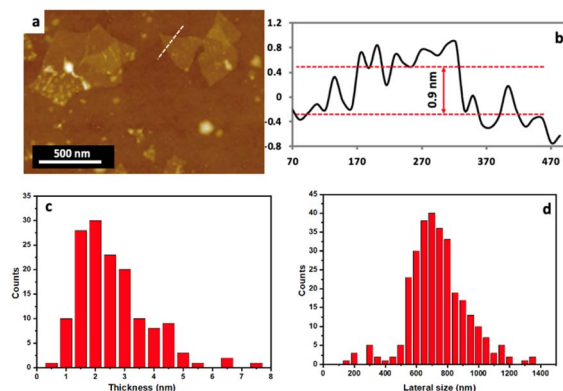


Fig. 4 (a and b) AFM image with its height profile of MoS<sub>2</sub> (c) layer thickness and (d) lateral size of exfoliated nanosheets synthesized using a VFD, under continuous flow at the optimised conditions.

Raman spectroscopy has been used to investigate structural characteristics of the exfoliated MoS<sub>2</sub> nanosheets obtained using VFD processing compared with that of the bulk material. The typical Raman spectra for MoS<sub>2</sub> materials shows two characteristic peaks, Fig. S6d,† the A<sub>1g</sub> and E<sub>2g</sub> modes, corresponding to the out-of-plane vibration of sulfur atoms and the in-plane vibration of Mo and sulfur atoms.<sup>28,29</sup> Fig. 5a shows the characteristic Raman spectrum of exfoliated MoS<sub>2</sub>, having a blue shift near 382 cm<sup>-1</sup> corresponding to the E<sub>2g</sub>, and 407 cm<sup>-1</sup> corresponding to the A<sub>1g</sub> active modes, which is consistent with the presence of exfoliated MoS<sub>2</sub> nanosheets. Furthermore, the peak shift indicates a decrease in the number of layers of MoS<sub>2</sub>.<sup>30,31</sup>

X-ray powder diffraction (XRD) of the exfoliated material confirmed the phase of MoS<sub>2</sub>, Fig. S6e,† with 2θ peaks at 14.4,

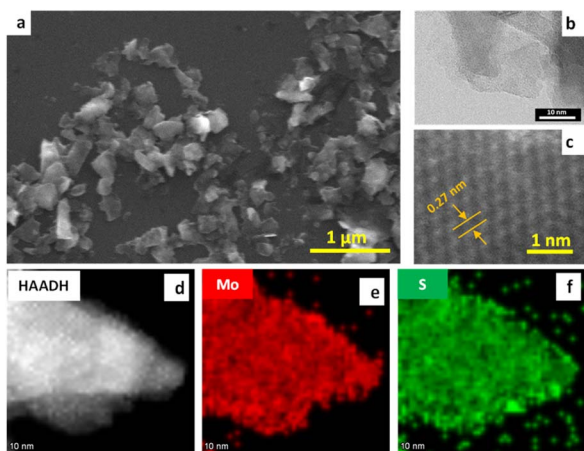


Fig. 3 SEM image (a), TEM and HRTEM images (b and c), STEM images (d–f) with elemental mapping, using a VFD, under continuous flow at the optimised conditions, using a 1 : 1 mixture of ethanol/water, under continuous flow conditions at a flow rate of 0.45 mL min<sup>-1</sup> and rotational speed 8k rpm.

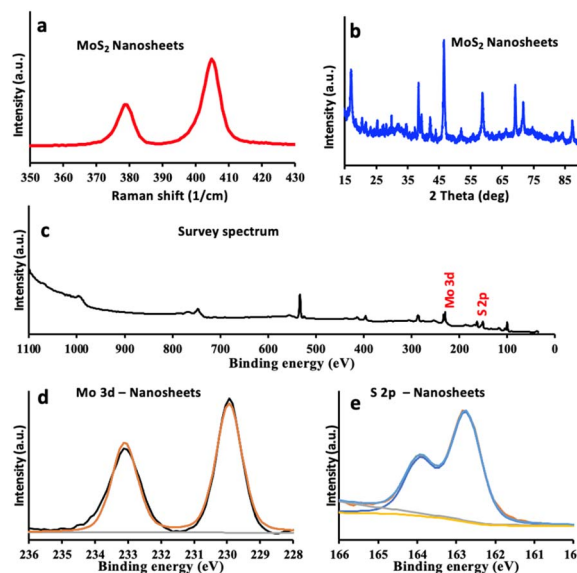


Fig. 5 (a) Raman spectra and (b) XRD patterns (c) survey XPS, (d and e) high-resolution spectra of Mo 3d and S 2p, for exfoliated MoS<sub>2</sub> nanosheets generated in the VFD under optimal processing conditions.



29.2, 32.6, 33.6, 36.0, 39.7, 44.7, 50.0, 58.5, 60.2, 72.2, 73.8 and 88.3° assigned to the (002), (004), (100), (101), (102), (103), (006), (105), (110), (008), (108), (203) and (118) planes of MoS<sub>2</sub>, respectively.<sup>32,33</sup> After exfoliation using the VFD, all peaks for molybdenite are present, Fig. 5b, however, the intensity of the (002) peak has decreased indicating that the exfoliated nanosheets are consistently very thin, down to a few layers.<sup>34,35</sup>

XPS was used for verifying the chemical composition of the bulk and exfoliated MoS<sub>2</sub>. Fig. 5c–e displays XPS survey spectrum and high-resolution scan for Mo 3d for both materials.<sup>36</sup> The XPS spectra of Mo 3d, for bulk MoS<sub>2</sub>, Fig. S6b,† has binding energies at ~233 eV and ~229 eV which correspond to Mo 3d<sub>3/2</sub> and Mo 3d<sub>5/2</sub> respectively.<sup>37</sup> After exfoliation to nanosheets, both Mo 3d<sub>3/2</sub> and Mo 3d<sub>5/2</sub> peaks are observed with the same positions at ~233 eV and ~229 eV, Fig. 5d. These peaks can be attributed to the 2H phase of MoS<sub>2</sub>. Fig. S6c† shows the high-resolution S 2p spectrum of both materials, for bulk MoS<sub>2</sub>, the S 2p peaks are located at low binding energies of ~162.2 eV corresponding to that for Mo–S bonds.<sup>36</sup> After exfoliation using the VFD, the S 2p<sub>3/2</sub> peak has similar pattern with no shift, Fig. 5e, which can also confirm that the exfoliated MoS<sub>2</sub> is resulting from the 2H phase and remain unoxidized.<sup>38</sup>

In summary, we have successfully employed the vortex fluidic device operating under ambient conditions and continuous flow processing to exfoliate MoS<sub>2</sub>. A significant benefit of this synthetic method is the potential for scaling up of production of the material while ensuring that the processing has environmentally sustainable credentials. In this method, 2D MoS<sub>2</sub> nanosheets are generated by the high shear associated with the spinning top topological fluid flow in the thin film in the VFD, impacting on the surface of the rapidly rotating tube. Also of note is that solutions of exfoliated MoS<sub>2</sub> prepared in the VFD are colloiddally stable over at least 3 months, Fig. S8,† and that the VFD is a relatively energy efficient processing device, as supported in the ESI file.†

## Author contributions

T. M. D. A. and C. L. R. designed the experiments, T. M. D. A. performed the experiments and carried out all SEM, TEM, HRTEM, XRD, Raman and XPS. T. M. D. A. and C. L. R. wrote the paper. All the authors approved the manuscript.

## Conflicts of interest

There are no conflicts to declare.

## Acknowledgements

The authors also thank Australian Research Council (DP200101105), The Government of South Australia, and AMF for support of this work. T. M. D. A. would like to thank Taibah University (Ministry of Education, Saudi Arabia) for help and support. TEM and HRTEM measurements were undertaken at Adelaide Microscopy, the Centre for Advanced Microscopy and Microanalysis. T. M. D. A. thanks Dr Ashley Slattery from Adelaide Microscopy for assistance with TEM and HRTEM imaging.

## Notes and references

- 1 A. Giri, G. Park and U. Jeong, *Chem. Rev.*, 2023, **123**, 3329–3442.
- 2 X. Zhu, Z. Su, C. Wu, H. Cong, X. Ai, H. Yang and J. Qian, *Nano Lett.*, 2022, **22**, 2956–2963.
- 3 R. Yang, Y. Fan, L. Mei, H. S. Shin, D. Voiry, Q. Lu, J. Li and Z. Zeng, *Nat. Synth.*, 2023, **2**, 101–118.
- 4 G. H. Han, D. L. Duong, D. H. Keum, S. J. Yun and Y. H. Lee, *Chem. Rev.*, 2018, **118**, 6297–6336.
- 5 L. Zheng, X. Wang, H. Jiang, M. Xu, W. Huang and Z. Liu, *Nano Res.*, 2022, 1–20.
- 6 S. Bellani, A. Bartolotta, A. Agresti, G. Calogero, G. Grancini, A. Di Carlo, E. Kymakis and F. Bonaccorso, *Chem. Soc. Rev.*, 2021, **50**, 11870–11965.
- 7 V. Kaushik, S. Wu, H. Jang, J. Kang, K. Kim and J. W. Suk, *Nanomaterials*, 2018, **8**, 587.
- 8 J. Zhou, Z. Lin, H. Ren, X. Duan, I. Shakir, Y. Huang and X. Duan, *Adv. Mater.*, 2021, **33**, 2004557.
- 9 Y. Zhao, Y. Yan and J.-M. Lee, *Nanoscale*, 2022, **14**, 1076–1095.
- 10 E. Varrla, C. Backes, K. R. Paton, A. Harvey, Z. Gholamvand, J. McCauley and J. N. Coleman, *Chem. Mater.*, 2015, **27**, 1129–1139.
- 11 X. Yin, Y. Li, W. Wu, G. Chu, Y. Luo and H. Meng, *Ind. Eng. Chem. Res.*, 2017, **56**, 4736–4742.
- 12 H. Yuan, X. Liu, L. Ma, P. Gong, Z. Yang, H. Wang, J. Wang and S. Yang, *RSC Adv.*, 2016, **6**, 82763–82773.
- 13 T. Alharbi, M. Jellicoe, X. Luo, K. Vimalanathan, I. K. Alsulami, B. S. A. Harbie, A. Igder, F. A. Alrashaidi, X. Chen and K. Stubbs, *Nanoscale Adv.*, 2021, **3**, 3064–3075.
- 14 M. Jellicoe, A. Igder, C. Chuah, D. B. Jones, X. Luo, K. A. Stubbs, E. M. Crawley, S. J. Pye, N. Joseph and K. Vimalanathan, *Chem. Sci.*, 2022, **13**, 3375–3385.
- 15 T. M. Alharbi, S. Elmas, A. S. Alotabi, M. R. Andersson and C. L. Raston, *ACS Sustainable Chem. Eng.*, 2022, **10**, 9325–9333.
- 16 T. Alharbi, K. Vimalanathan, I. Alsulami and C. L. Raston, *Nanoscale*, 2019, **11**, 21394–21403.
- 17 T. M. Alharbi, Q. Li and C. L. Raston, *ACS Sustainable Chem. Eng.*, 2021, **9**, 16044–16051.
- 18 S. Lin, X. Chen and Z. L. Wang, *Chem. Rev.*, 2021, **122**, 5209–5232.
- 19 L. Chen, Q. Shi, Y. Sun, T. Nguyen, C. Lee and S. Soh, *Adv. Mater.*, 2018, **30**, 1802405.
- 20 X. Chen, J. F. Dobson and C. L. Raston, *Chem. Commun.*, 2012, **48**, 3703–3705.
- 21 A. H. M. Al-Antaki, X. Luo, T. M. Alharbi, D. P. Harvey, S. Pye, J. Zou, W. Lawrance and C. L. Raston, *RSC Adv.*, 2019, **9**, 22074–22079.
- 22 M. Batmunkh, K. Vimalanathan, C. Wu, A. S. Bati, L. Yu, S. A. Tawfik, M. J. Ford, T. J. Macdonald, C. L. Raston and S. Priya, *Small Methods*, 2019, **3**, 1800521.
- 23 X. Chen, R. A. Boulos, J. F. Dobson and C. L. Raston, *Nanoscale*, 2013, **5**, 498–502.



- 24 B. Adilbekova, Y. Lin, E. Yengel, H. Faber, G. Harrison, Y. Firdaus, A. El-Labban, D. H. Anjum, V. Tung and T. D. Anthopoulos, *J. Mater. Chem. C*, 2020, **8**, 5259–5264.
- 25 G. Gao, C. Chen, X. Xie, Y. Su, S. Kang, G. Zhu, D. Gao, A. Trampert and L. Cai, *Mater. Res. Lett.*, 2017, **5**, 267–275.
- 26 G. Eda, H. Yamaguchi, D. Voiry, T. Fujita, M. Chen and M. Chhowalla, *Nano Lett.*, 2011, **11**, 5111–5116.
- 27 Z. Yin, H. Li, H. Li, L. Jiang, Y. Shi, Y. Sun, G. Lu, Q. Zhang, X. Chen and H. Zhang, *ACS Nano*, 2011, **6**, 74–80.
- 28 W. Han, Y. Xia, D. Yang and A. Dong, *Chem. Commun.*, 2021, **57**, 4400–4403.
- 29 X. Wu, Y. Li, L. Chen, J. Zhao, B. Wu and Z.-B. Zhang, *Chem. Commun.*, 2020, **56**, 2035–2038.
- 30 Z. Mohammadpour, S. H. Abdollahi and A. Safavi, *ACS Appl. Energy Mater.*, 2018, **1**, 5896–5906.
- 31 H. Li, Q. Zhang, C. C. R. Yap, B. K. Tay, T. H. T. Edwin, A. Olivier and D. Baillargeat, *Adv. Funct. Mater.*, 2012, **22**, 1385–1390.
- 32 V. Štengl and J. Henych, *Nanoscale*, 2013, **5**, 3387–3394.
- 33 Q. Yang, Z. Wang, L. Dong, W. Zhao, Y. Jin, L. Fang, B. Hu and M. Dong, *J. Phys. Chem. C*, 2019, **123**, 10917–10925.
- 34 Y. Li, X. Yin and W. Wu, *Ind. Eng. Chem. Res.*, 2018, **57**, 2838–2846.
- 35 D. Sahoo, B. Kumar, J. Sinha, S. Ghosh, S. S. Roy and B. Kaviraj, *Sci. Rep.*, 2020, **10**, 1–12.
- 36 J. Guo, H. Zhu, Y. Sun, L. Tang and X. Zhang, *Electrochim. Acta*, 2016, **211**, 603–610.
- 37 D. Qi, S. Li, Y. Chen and J. Huang, *J. Alloys Compd.*, 2017, **728**, 506–517.
- 38 Q. D. Truong, M. Kempaiah Devaraju, Y. Nakayasu, N. Tamura, Y. Sasaki, T. Tomai and I. Honma, *ACS Omega*, 2017, **2**, 2360–2367.

